Journal Pre-proofs

Modelling of a recirculating photocatalytic microreactor implementing mesoporous N-TiO_2 modified with graphene

Ahmed Yusuf, Habeebllah Oladipo, Lütfiye Yildiz Ozer, Corrado Garlisi, Vittorio Loddo, Mohammad R.M. Abu-Zahra, Giovanni Palmisano

PII: S1385-8947(19)32989-4
DOI: https://doi.org/10.1016/j.cej.2019.123574
Reference: CEJ 123574

To appear in: *Chemical Engineering Journal*

Received Date: 1 May 2019
Revised Date: 17 September 2019
Accepted Date: 19 November 2019

Please cite this article as: A. Yusuf, H. Oladipo, L. Yildiz Ozer, C. Garlisi, V. Loddo, M.R.M. Abu-Zahra, G. Palmisano, Modelling of a recirculating photocatalytic microreactor implementing mesoporous N-TiO_2 modified with graphene, *Chemical Engineering Journal* (2019), doi: https://doi.org/10.1016/j.cej.2019.123574

Modelling of a recirculating photocatalytic microreactor implementing mesoporous N-TiO_2 modified with graphene

Ahmed Yusuf,[1,2] Habeebllah Oladipo,[1,3] Lütfiye Yildiz Ozer,[1,2] Corrado Garlisi,[1] Vittorio Loddo,[4] Mohammad R.M. Abu-Zahra,[1,3] Giovanni Palmisano[1,2,3]

[1]Department of Chemical Engineering, Khalifa University of Science and Technology, P.O. Box 135125, Abu Dhabi, United Arab Emirates

[2]Center for Membrane and Advanced Water Technology, Khalifa University of Science and Technology, P.O. Box 135125, Abu Dhabi, United Arab Emirates

[3] Research and Innovation Center on CO_2 and H_2, Khalifa University of Science and Technology, P.O. Box 135125, Abu Dhabi, United Arab Emirates

[4] Department of Engineering (DI), "Schiavello-Grillone" Photocatalysis Group - Università degli Studi di Palermo, Viale delle Scienze, 90128 Palermo, Italy

E-mail: giovanni.palmisano@ku.ac.ae

Abstract

The use of microreactors in (photo)catalytic processes offers new possibilities for studying and optimizing many mass and photon transfer limited reactions. In this study, we propose a scalable computational fluid dynamics (CFD) model for the prediction of photocatalytic degradation of a model pollutant (4-nitrophenol) using immobilized N-doped TiO_2 grown over reduced graphene oxide (N-TiO_2/rGO) in a photocatalytic microreactor working in continuous flow-recirculation mode. The mode of operation used in this study allows the reduction of mass transfer limitations inherent to heterogeneous photocatalytic reactions taking place on immobilized catalysts. A CFD model was developed for effective prediction of experimental results using COMSOL multi-

physics. The experiment and the model results clearly showed a good agreement. The model parameters were determined through fitting the model with the experimental data, adsorption rate constants were estimated to be 1.76x10^4 m^3 mol^{-1} h^{-1} and 0.0252 h^{-1} for monolayer ($k_{ads,m}$, and $k_{des,m}$), 1.76x10^4 m^3 mol^{-1} h^{-1} and 0.0126 h^{-1} for multilayer ($k_{ads,n}$, and $k_{des,n}$); and the intrinsic rate constant (k_s) was 2.02 h^{-1}. This proposed model herein could serve as a practical tool to improve and optimize an extensive number of photocatalytic reactions for (waste)water applications in microreactors operating in recirculation mode.

Keywords: microreactor; photocatalysis; total recirculation; CFD modelling

Nomenclature

Parameter	Unit	Description
C	mol m^{-3}	Bulk concentration of 4-nitrophenol
C_0	mol m^{-3}	Initial concentration of 4-nitrophenol
C_s	mol m^{-2}	Adsorbed 4-nitrophenol per unit surface
C_{eq}	mol m^{-3}	4-nitrophenol concentration at equilibrium
C_t	mol m^{-3}	Concentration of 4-nitrophenol in the tank
C_{exit}	mol m^{-3}	Average concentration of 4-nitrophenol leaving the microreactor exit
D	m^2 s^{-1}	Diffusivity of 4-nitrophenol in bulk
D_s	m^2 s^{-1}	Surface diffusivity of 4-nitrophenol
Da_I	Dimensionless	Damkohler number I
Da_{II}	Dimensionless	Damkohler number II
F	N m^{-3}	Generic body forces
h	m	Microchannel height and width
I	-	Identity matrix
K	m^{-3} mol^{-1}	Adsorption-desorption equilibrium constant
κ	m^{-1}	Illuminated catalyst surface

k_s	h^{-1}	Intrinsic rate constant
k_{app}	mol m^{-3} h^{-1}	Apparent rate constant
$k_{ads,\ m}$	m^3 mol^{-1} h^{-1}	Adsorption rate constant in monolayer
$k_{des,\ m}$	h^{-1}	Desorption rate constant in monolayer
$k_{ads,\ n}$	m^3 mol^{-1} h^{-1}	Adsorption rate constant in multilayer
$k_{des,\ n}$	h^{-1}	Desorption rate constant in multilayer
L	cm	Microchannel length
M	-	monolayer
N	-	multilayer
Pe	Dimensionless	Peclet number
Q	cm^3 h^{-1}	Recirculation flowrate to and from the microreactor
R	-	Sum of squares of residuals
R *(dark, light)*	mol m^{-2} h^{-1}	Reaction rate for dark adsorption or degradation
R_s	mol m^{-3} h^{-1}	Rate of degradation under irradiation
R_{ads}	mol m^{-2} h^{-1}	Net rate of adsorption on the catalyst surface
$R_{ads,\ m}$	mol m^{-2} h^{-1}	Net rate of adsorption on monolayer
$R_{ads,\ n}$	mol m^{-2} h^{-1}	Net rate of adsorption on multilayer
Re	-	Reynolds number
S	-	The vacant site on photocatalyst for adsorption
t_D	s	Diffusion time in fluid
t_R	s	Residence time in microreactor
t_k	s	Reaction time
t	h	Time
t_s	s	Space time
t_{eq}	h	Adsorption equilibrium time
V_t	m^3	Volume of total 4-nitrophenol solution in the tank
V_R	cm^3	Total Volume of the microreactor
y_{exp}	-	Experimental output
y_{model}	-	Model output
ρ	kg m^{-3}	Density
U	m s^{-1}	Velocity vector
p	Pa	Pressure
Γ	mol m^{-2} or mmol (g-catalyst) $^{-1}$	Monolayer adsorption capacity or maximum adsorption capacity
μ	g m^{-1} s^{-1}	Dynamic viscosity
T'	-	Transpose operator

1. Introduction

Heterogeneous photocatalysis (HPC) continues to gain major attention as an elective advanced oxidation technique in a number of environmental protection applications, including degradation of recalcitrant and emerging organic molecules or micropollutants [1,2]. One of the major setbacks limiting large-scale deployment of photocatalytic processes is the reaction environment. Slurry reactors are the conventional photo-reactors used for studying photocatalytic reactions at laboratory and pilot scales. These photocatalytic reactors are normally stymied by low photonic efficiency due to non-uniform distribution of light in suspension, mass transfer limitation resulting from slow diffusion, and extra cost associated with photocatalyst separation from the reaction medium. Notably, immobilization of photocatalysts on substrates, such as glass [3,4], represents an effective strategy to avoid additional cost related to the catalyst recovery. Despite the undoubted advantages of this approach, reduced exposed photocatalyst surface area and difficult scale-up are severe setbacks of this configuration [5]. In this context, microreactor technology has the potential to overcome the intrinsic limitations associated with slurry and conventional immobilized photocatalytic macro-reactors [6].

Remarkable features of microreactors are mainly due to the smallness and compactness of their reaction environment, with at least one dimension in few micrometres. They ensure high surface-to-volume ratio, short molecular diffusion distances, superior mass and heat transfer features and good laminar flow. In HPC, these attractive features translate to higher spatial illumination uniformity and permeation through the entirety of microreactor compared to macro-reactors [7,8].

While many studies have been carried out on the application of microreactors in HPC, only very few have addressed modelling aspects, being fundamental for a successful scale-up of

micro-structured devices. One of the few studies in this area was carried out by Charles et al. [9] who modelled the photodegradation of salicylic acid over immobilized TiO_2 photocatalyst as a function of rectangular microchannel size, pollutant concentration, flow rate and incident UV light intensity. They observed higher degradation at low initial salicylic acid concentration and low flow rates. They also reported and validated a simple and rapid approach for the determination of the reaction rate constant. Elsewhere, Corbel et al. [10] extended the previous work of Charles et al. by CFD modelling and investigated the dependence of photodegradation of salicylic acid with varying microreactor configurations and flowrates. They found that the microreactor with the shallowest depth and highest specific surface area exhibited the best photocatalytic activity. In another work by Corbel et al. [11], the influence of mass transfer at low flowrates on photocatalytic efficiency was investigated through CFD modelling, which was validated with experimental data. They developed a simple correlation for mass transfer coefficient that can sufficiently define experimental results for Reynolds number between 1 and 4. Recently, Corbel et al. [12] had also reported a kinetic study on the photocatalytic degradation of Ifosfamide in microchannel immobilized with ZnO sensitized quantum dots at low flow rate in a continuous flow mode using CFD modelling. Their estimation of Sherwood and average Damkohler number for experimental results revealed that the photocatalytic reaction is limited by mass transfer. To the best of our knowledge, most of the previous modelling studies on microreactors using immobilized photocatalysts have only carried out their investigation (i) at low flow rates which still brings about some mass transfer limitations, (ii) in continuous flow mode without recirculation, (iii) using bare TiO_2 and other inorganic semi-conductor photocatalyst such as ZnO, and (iv) not accounting for dark stage adsorption in their models.

This study presents the first investigation on CFD modelling of a photocatalytic degradation carried out in a parallel microreactor channels configuration with immobilized porous N-TiO_2/reduced graphene oxide nanocomposites (N-TiO_2/rGO) in continuous flow-recirculation mode. The probe pollutant was 4-nitrophenol dissolved in water, whose photocatalytic degradation was carried out in a microreactor irradiated by simulated solar light, using a novel photocatalyst recently developed in a powder form by our group [13]. Unlike previous works, this study was performed at high recirculation flow rate, thus eliminating the effects of mass transfer limitations. Moreover, the modelling aspect accounted for dark stage adsorption, which is an additional novelty of this work. The present study shows how the unique features of the microreactor technology coupled with the tremendous properties of graphene-based photocatalysts provide a solid basis for the improvement and optimization of photocatalytic processes, thereby making them the preferred option for increasingly efficient and safe wastewater treatment.

2. Experimental

2.1 Preparation of the film

Nitrogen-doped TiO_2 grown on reduced graphene oxide was synthesized by sol-gel method as mentioned in our previous works [13,14]. The film was deposited by spin coating using a 4 cm^3 suspension containing: 128 mg of catalyst, 2.61 cm^3 of ethanol, 83.88 µl of Triton X-100 and 0.13 µl of nitric acid. The suspension was dropped on a glass substrate (8 by 8 cm with thickness of 0.8 cm) and rotated at 500 rpm for 3 s during the deposition. The film was dried on a hot plate at 60 ^oC for 45 min followed by cooling down to room temperature. After deposition, the film was

annealed in nitrogen flow according to the following steps: heating up to 50°C in 30 min, heating up from 50°C to 450°C in 6 h and stay 4 h at 450°C. The sample was then allowed to cool down below 200°C under nitrogen flow.

2.2 Characterization

Raman spectroscopy was used to identify the crystal phase of the prepared film and was carried out in a confocal Raman spectroscope (Alpha 300R from Witec). The sample was excited with 532 nm laser having a single mode output power of 52 mW. Focus Ion Beam Scanning Electron Microscope (FIB-SEM, Helios NanoLab) was used to study the morphology of the sample. The XRD could not be carried out with sample on the glass but we have provided the XRD analysis for the powdered sample in the supporting information (see Figure S1).

2.3 Modelling and Evaluation of photocatalytic activity

The photocatalytic activity of the immobilized catalyst under simulated solar irradiation towards 4-nitrophenol degradation was carried out in a microreactor operating under recirculation mode. The microreactor consists of nine Microchannels each with a square cross-section of edge 0.05 cm and length of ca. 5 cm connected in parallel. Table 1 shows the flow and geometric properties of one microchannel, the effective hydraulic diameter and the Re number were estimated according to the method reported in ref [15]. The space time (t_s) was estimated by dividing the volume of one microchannel by the volumetric flow rate. The small value of Re number confirms that the flow inside the microchannel is laminar.

Table 1. Microchannel flow characteristics (396 cm^3 h^{-1}) and dimension.

Width/depth (*h*) (cm)	Length (*L*) (cm)	Volume (cm^3)	Estimated space time (t_s) (s)	Estimated Mean velocity (cm/s)	Effective hydraulic diameter (cm)	*Re* number
0.05	5	0.0125	0.114	3.75	0.0562	21.1

The irradiation source employed uses a LOT Quantum Design LS0606, equipped with a 1000 W Xenon short arc lamp and an AM1.5G Filter (see Figure S2 for the emission spectra of this solar irradiation simulator). The average values of the radiation on the film surface were 8.5 and 710 W m^{-2} in the ranges of 315-400 and 450-950 nm, measured with a Delta Ohm 9721 radiometer. The transmittance of the silicone template measured in the UV (315-400nm) and visible (450-950nm) range were 50% and 91% respectively. This means that silicone screens out half UV radiation of the simulated solar light. The total illuminated catalytic surface area per unit of liquid treated inside the reactor, κ, is an important photocatalytic reactor design parameter. For the microreactor used in this study, the illuminated photocatalyst density is about 2000 m^{-1}, this value is lower compared to 11667 m^{-1} reported by ref. [4]: this disparity was due to the lower photocatalyst coated area and to the different cross-sectional area of the microchannel. In this study, eq. 1 was used to estimate the parameter, κ.

$$\kappa = \frac{1}{h} \quad (1)$$

where κ (m^{-1}) is the illuminated catalyst surface area and h (m) is the height (or width) of the square microchannels. We assumed that only the catalytic surface area in contact with the 4-nitrophenol solution contributed to the photo-reactivity. In the microreactor, only the glass side

of each microchannel has the deposited N-TiO_2/rGO film (Figure 1). We believe that the capillary action or forces in the microreactor are minimal because the silicone microchannel template was tightly screwed against the photocatalytic film on the glass using a torque of 0.5 Nm. In addition, the flow in the microreactor is controlled by a peristaltic pump connected to the recirculation tank which contains both the exit and inlet lines.

For each experimental run, 125 cm^3 of 4-nitrophenol solution (starting concentrations of 0.0323, 0.0518, 0.134, 0.324 mol m^{-3}) was charged into a recirculation tank. The 4-nitrophenol solution in the tank was fed into the microreactor through a peristaltic pump set to a flowrate of 396 cm^3 h^{-1} while effluent from the same microreactor was returned back to the tank. The flowrate was chosen based on preliminary hydrodynamic studies performed (see Figure S3 in the Supporting Information) to minimize the external diffusion limitations by working at a sufficient flowrate. Figure 1 depicts all the essential components of the microreactor which was home-made.

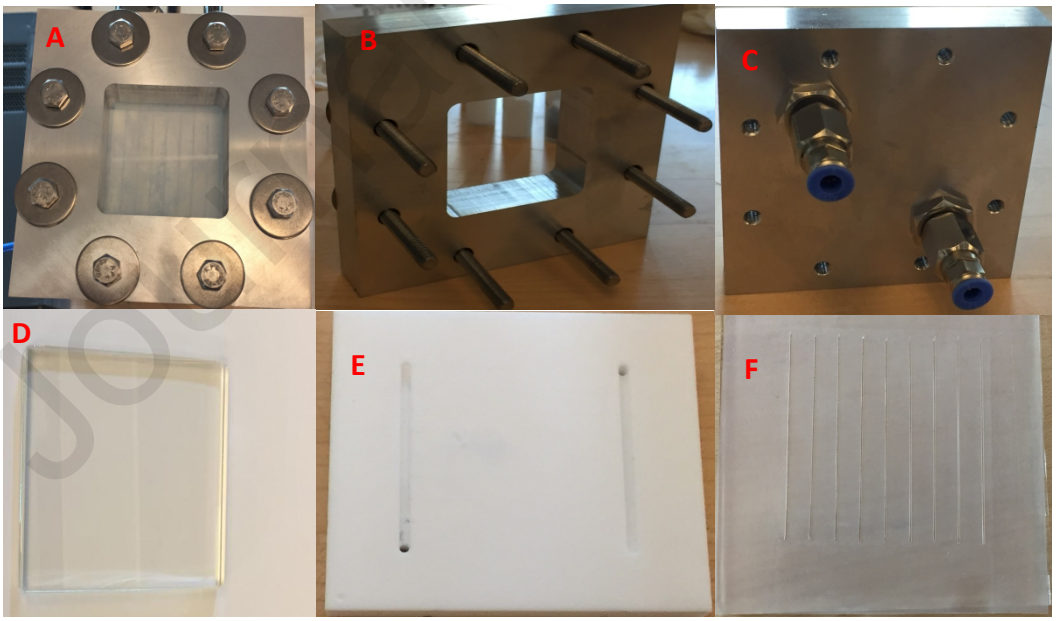

Figure 1. Components of the microreactor used in the experimental set up: **(A)** top view of the photocatalytic microreactor, **(B)** top casing that houses the microreactor, **(C)** bottom casing

showing inlet and outlet, **(D)** glass substrate where the catalyst was immobilized, **(E)** PTFE template (directly connected to C) showing both inlet and outlet, **(F)** silicone microchannels template (each channel measures 0.05 cm by 0.05 cm by 5cm) showing all nine microchannels.

The contents of the recirculation tank was kept under stirring to ensure uniform 4-nitrophenol concentration within at all time. Initially, experiments were performed in the dark until the adsorption-desorption equilibrium was established. Liquid samples were intermittently withdrawn from the recirculation tank, filtered with a 0.2 µm PTFE filter and analysed with Dionex UlitMate 3000 ThermoScientific High Performance Liquid Chromatography (HPLC). Absorbance at 315 nm was used to evaluate the removal of 4-nitrophenol from solution. At the end of an experimental run, the catalyst was regenerated by flowing DI water (18.6 MΩ) through the microreactor under irradiation. This regeneration was facile and was carried out without uncoupling the immobilized catalyst from the microreactor system.

COMSOL Multiphysics version 5.2© software has been used for numerically solving the model developed for this experiment. This software utilizes the finite element method (FEM) to obtain numerical solutions of model equations. Specifically, the chemical engineering module was used for simulating the chemical reaction related models. This module contains nodes that describe the transport of both dilute and concentrated species. In this work, the node for transport of diluted species has been used to model the transport of 4-nitrophenol through the microchannels.

The fitting of experimental data to model results was carried out using the optimization node of COMSOL Multiphysics. The fitting of model was based on minimization of the sum of squares of residuals (see eq. (2)). The optimization node is equipped with simultaneous parameter

estimation in which the unknown model parameter that best fits experimental result can be obtained.

$$R = \sum_{i}^{n} (y_{exp} - y_{model})^2 \quad (2)$$

where *R* is the sum of the squares of residuals to be minimized, y_{exp} is the experimental result and y_{model} is the model result to be validated. The fitting was performed separately for the dark and the light stages of the experiments.

3. Results and Discussion

3.1 Morphological and structural characterization

Raman signals, shown in Figure 2A, were clearly observed for brookite at: 127, 146, 246, 402 and 638 cm^{-1} assigned to A_{1g} mode, 323 cm^{-1} due to B_{1g} mode, 366 and 451 cm^{-1} ascribed to B_{2g} mode [16]. The bands at 146, 451 and 638 cm^{-1} are indicative of A_{1g}, E_{1g} and B_{1g} modes of rutile phase [17]. Raman signal at 518 cm^{-1} probably derives from either trace of anatase phase (A_{1g} mode) or some residual organic impurity in the film. However, a rigorous identification of rutile bands and, to a greater extent, of anatase ones is not straightforward owing to the overlap with brookite signals. Raman signals of graphene did not appear in the spectrum due to its small amount used in catalyst preparation and strong background signal of TiO_2 [18].

Figure 2B shows the top view and the cross-sectional SEM images of the N-TiO_2/rGO film, which exhibited a highly macro-mesoporous structure. High porosity usually has a beneficial effect on the photocatalytic performance of microreactor devices due to the reduced diffusion resistance and upsurge in the average number of active sites per unit of surface. The overall thickness of the sample was 1 - 1.1 µm and two layers of about half a micron each stood out

clearly: (i) the bottom layer exhibiting a larger number of smaller pores with size up to ca. 100 nm; (ii) the top layer showing a more compact structure punctuated by a limited number of larger pores (up to 300 nm).

(A)

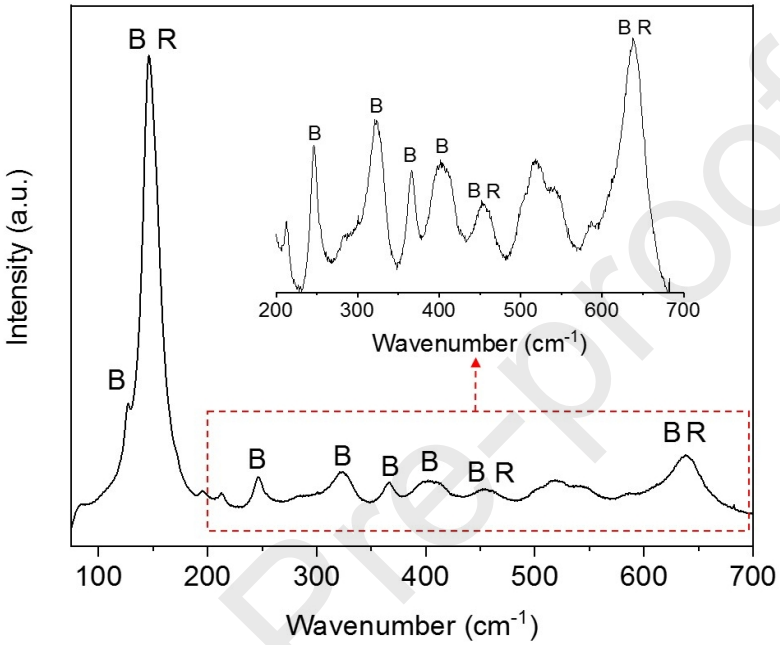

(B)

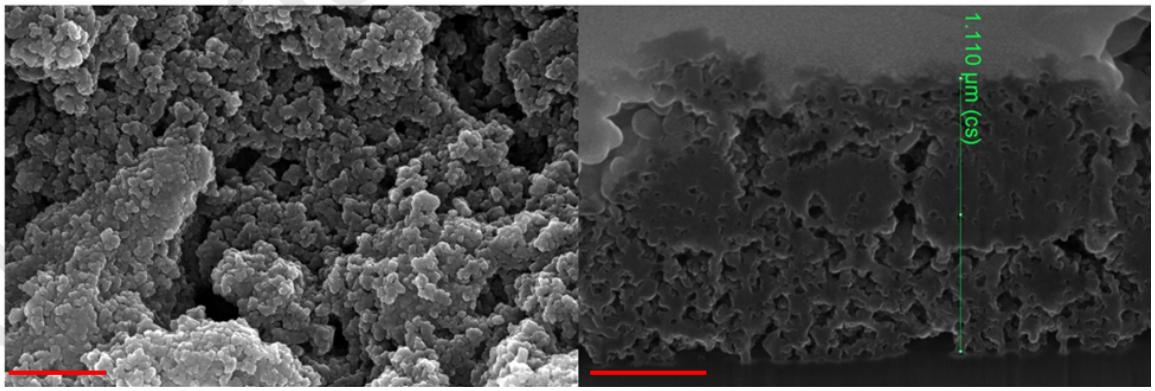

Figure 2. (A) Raman spectrum of the same sample (B: brookite and R: rutile). (B) Top view (left) and cross-sectional (right) SEM images of N-doped TiO_2 grown on reduced graphene oxide film on glass. The scale bar is 500 nm in both pictures.

3.2 Dark Adsorption and Degradation of 4-nitrophenol

The 4-nitrophenol concentration versus time, under dark conditions, at different initial concentration (C_o: 0.0323, 0.0518, 0.134, 0.324 mol m^{-3}) are depicted in Figure 3. In dark conditions, adsorption equilibrium was reached in the range of 180 – 312 h for all C_o. The adsorption in the dark in this study is significant, and it is due to the highly porous N-TiO_2/rGO film. With compact non porous films the dark adsorption is always minor or negligible. All tested C_o showed similar trend in 4-nitrophenol adsorption in dark conditions with sharp initial decline in the concentration of 4-nitrophenol. The nature of adsorption of 4-nitrophenol on N-TiO_2/rGO film was investigated using Langmuir adsorption isotherm. The linearized forms of both non-dissociative and dissociative adsorption models of Langmuir are represented in eq. (3) and (4) [19], and they were used to fit the obtained experimental data.

$$\frac{1}{C_s} = \frac{1}{KC_{eq}\Gamma} + \frac{1}{\Gamma} \quad (3)$$

$$\frac{1}{C_s} = \frac{2}{\Gamma} + \frac{1}{\Gamma(KC_{eq})^{0.5}} \quad (4)$$

where C_s (mol m^{-2}) and C_{eq} (mol m^{-3}) represent the concentration of adsorbed 4-nitrophenol species and equilibrium concentration of 4-nitrophenol, Γ (mol m^{-2}) is the maximum adsorption capacity and K (m^3 mol^{-1}) is the adsorption-desorption equilibrium constant. A plot of the eq. 3 resulted in a negative value of Γ, both in the case of dissociative and non-dissociative adsorption.

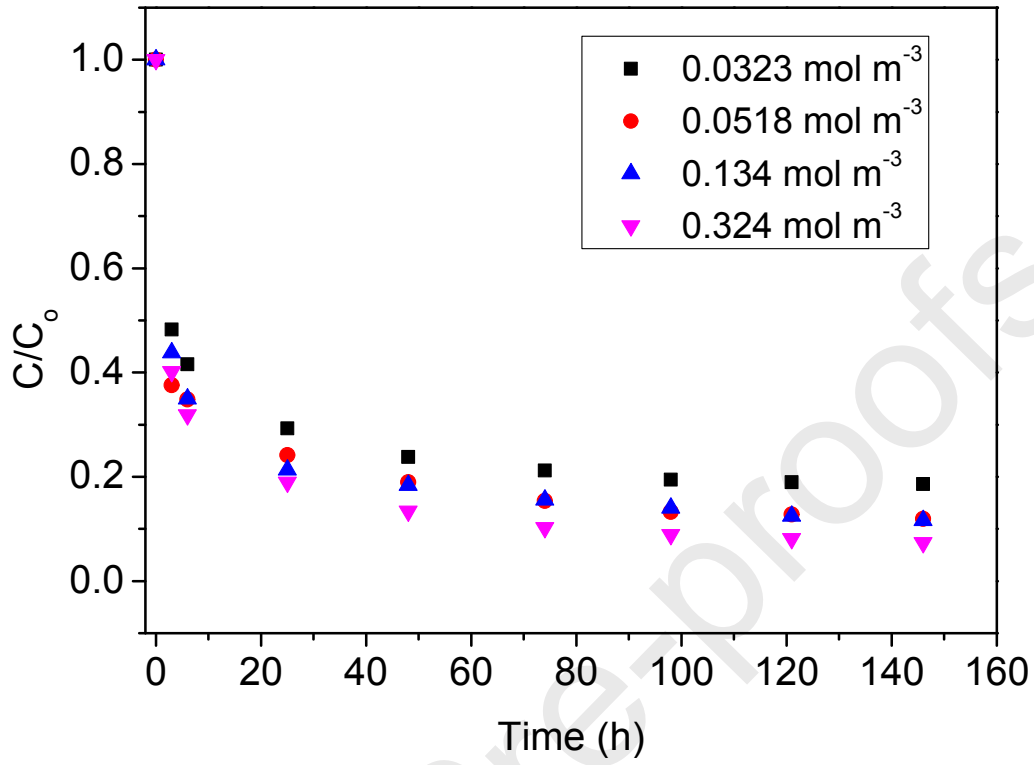

Figure 3. Comparison of 4-nitrophenol disappearance in the dark at different starting concentrations.

Therefore, it can be concluded that the adsorption of 4-nitrophenol on the N-TiO_2/rGO film is not monolayer in nature but physical and multilayer, explaining why the Langmuir model fails to predict the adsorption kinetics. Our previous study on N-TiO_2/rGO photocatalyst used in slurry reactor shows negligible adsorption in the dark phase [13]. The enhanced adsorption capacity found in this study is a combined effect of the properties of both the microreactor and high porosity of the N-TiO_2/rGO film. The microreactor setup, in fact, ensures a shorter diffusion path between the catalytic sites and 4-nitrophenol species in the bulk.

After the dark adsorption, the degradation of 4-nitrophenol was carried out under solar simulator. A slight increase in the 4-nitrophenol concentration in the recirculating tank was observed soon after the light was switched on. This observation confirmed a slight photo-desorption of the pollutant, which has been widely reported in the literature [20,21]. The decrease in 4-nitrophenol concentration was observed to follow a zero-order kinetics. The estimated apparent observed rate constant for all initial concentration of 4-NP used are summarized in Table 2. Moreover, additional degradation experiments were carried out without any initial dark phase adsorption. In such cases the concentration of 4-nitrophenol in the recirculating tank was observed to be always higher with respect to an analogous experiment where dark phase adsorption had preceded illumination (see Figure S4 in supporting information).

Table 2. Relationship between equilibrium concentration and observed rate of photocatalytic degradation.

C_o (mol m^{-3})	C_{eq} (mol m^{-3})	$-R_s = k_{app}$ (mol m^{-3} h^{-1})	$k_{app}/C_{eq} = k_s$ (h^{-1})
0.0323	0.00578	0.00832	0.00200
0.0518	0.00534	0.00728	0.00190
0.134	0.0122	0.0182	0.00210
0.324	0.0164	0.0213	0.00180

There is a direct relationship between the equilibrium concentrations (C_{eq}) and the reaction rate constant (see Table 2) because of the small concentration of 4-nitrophenol remaining after dark adsorption. Hence, the rate constant of photodegradation is given by eq. (5):

$$k_{app} = k_s C_{eq} \quad (5)$$

where k_{app} is the apparent rate constant in mol m^{-3} h^{-1}, and k_s is the intrinsic rate constant in h^{-1}.

It should be noted that, contrary to slurry systems, the microreactor system made it possible to have a simplified equation for photocatalytic degradation of 4-nitrophenol, partly due to the fact that photocatalytic rate constant does not depend on the starting concentration of the pollutant.

Table 3 shows the characteristic time scales and the dimensionless numbers. The relative significance of the reaction and transport processes taking place in the microreactor was evaluated from their approximate respective time scales. The Peclet (192) and Damkohler numbers I and II (1.77×10^{-7} and 1.4×10^{-4}) showed in Table 3 confirm that our experiment is not limited by diffusional resistances, but limited by kinetics thereby leading to higher reaction times. This was confirmed by a recent study by Satuf et al. [22], which reported a plot of Peclet against Damkohler numbers in order to determine the operating region of their microreactor. The same plot was used to confirm that our microreactor falls in the no diffusional limitations-kinetic control-very low conversion region.

Table 3. Characteristics time scales and dimensionless numbers [22].

Description	Symbol	Equation	Estimated value

Residence time	t_R	V_R/Q	1.3 s
Diffusion time in the fluid	t_D	h^2/D	250 s
Reaction time	t_k	$1/k_s$	500 h
Peclet Number	Pe	t_D/t_R	192
Damkohler I number	Da_I	t_R/t_k	7.22 x 10^{-7}
Damkohler II number	Da_{II}	t_D/t_k	1.4 x 10^{-4}

(V_R = 0.029 cm^3, Q = 396 $cm^3\ h^{-1}$, h = 0.05 cm, D = 10^{-9} $m^2\ s^{-1}$)

3.3 Validation of Experimental data with microreactor model (CFD)

3.3.1 Dark Adsorption and degradation

The photodegradation of 4-nitrophenol solution in a photocatalytic microreactor has been modelled by considering two steps: a dark stage where 4-nitrophenol species in bulk were adsorbed onto the photocatalyst surface until equilibrium was reached, followed by the degradation of surface-bound 4-NP species in the presence of light (simulated solar irradiation). Based on the experimental results, it was concluded that the adsorption was a multilayer process; therefore the monolayer-multilayer adsorption (MMA) model reported by Scheufele et al. [23] was adapted in this study. MMA model (see eq. (6)-(10)) assumes that the adsorption of the substrate takes place in two different active sites, which include the monolayer adsorption that is intrinsic to the surface of the adsorbent material. Multilayer adsorption due to adsorbate layers acting as active adsorption sites.

Monolayer adsorption:

$$C + S \overset{R_{ads,\ m}}{\longleftrightarrow} C_S \qquad (6)$$

n^{th} adsorption layer:

$$C + C_{S_{n-1}} \overset{R_{ads,\,n}}{\longleftrightarrow} C_{S,\,n} \quad (7)$$

$$R_{ads} = R_{ads,m} + R_{ads,n} \quad (8)$$

$$R_{ads,m} = -k_{ads,m} C (\Gamma - C_S) + k_{des,m} C_S \quad (9)$$

$$R_{ads,n} = -k_{ads,n} C\, C_S + k_{des,n} (C_S - \Gamma) \quad (10)$$

where $R_{ads,\,n}$ (mol m^{-2} h^{-1}) is rate of adsorption on n > 1 layer, $R_{ads,\,m}$ (mol m^{-2} h^{-1}) is the rate of adsorption on monolayer (n = 1) and R_{ads} (mol m^{-2} h^{-1}) is the total adsorption rate on monolayer-multilayer. C is the bulk concentration of 4-nitrophenol in mol m^{-3}, $k_{ads,\,m}$ is the monolayer adsorption rate constant in m^3 mol^{-1} h^{-1}, $k_{des,\,m}$ is the monolayer desorption rate constant in h^{-1}, $k_{ads,\,n}$ is the multilayer adsorption rate constant in m^3 mol^{-1} h^{-1}, $k_{des,\,n}$ is the multilayer desorption rate constant in h^{-1}.

The degradation rate of 4-nitrophenol under simulated solar irradiation (R_s) was first order with respect to C_{eq}. The degradation rate is an approximation of Langmuir-Hinshelwood model at very small bulk concentration which suits our experimental results. Therefore, the rate of degradation can be expressed according to eq. (11)-(12):

$$C_S \overset{R_S}{\rightarrow} \text{degradation products} \quad (11)$$

$$R_s = -k_s C_{eq} \quad (12)$$

3.3.2 Transport equations governing the CFD model

This CFD model utilized a two-dimensional domain of photocatalytic microreactors with nine parallel microchannels. The model was designed as a pseudo batch-mode operation where the outlet stream was recirculated back into the inlet to ensure multiple passes of the 4-nitrophenol solution (Figure 4A). Figure 4B depicts the model geometry used for the simulation in COMSOL Multiphysics©. The microreactor has nine microchannels with channel length of ca. 5 cm and square cross-section of edge 0.05 cm. The 2D domain employed had eleven domains with two of them serving as collectors (0.1 cm in width) and the remainders were the microchannels having one of the walls (with red colour in Figure 4B) with immobilized thin film of N-TiO_2/rGO. The inlet and outlet of the whole microreactor configuration were connected to a recirculating tank where the 4-nitrophenol solution is stored under constant stirring for multiple passes (see Figure 4A). The general assumptions made for the model are summarized as follows:

- 4-nitrophenol solution is dilute and incompressible and physical properties of water were assumed.
- Laminar flow was assumed in the whole microreactor configuration since *Re* is about 21.
- Effects of the capillary force was assumed to be negligible in the microchannels.
- Adsorption and degradation of 4-nitrophenol only took place on the side with N-TiO_2/rGO film in the microchannels.

The flow in the microreactor is laminar and the velocity component perpendicular to the catalytic side is assumed to be zero, while the component parallel to the catalytic side follows a gaussian distribution. The fluid flow was simulated at steady state and the resulting velocity vector was exported into the 4-nitrophenol species transport equations.

(A)

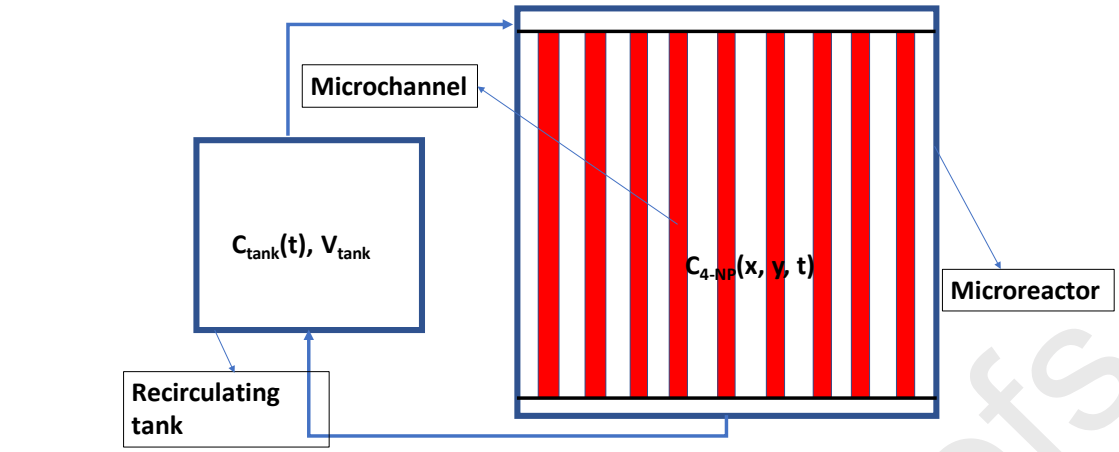

(B)

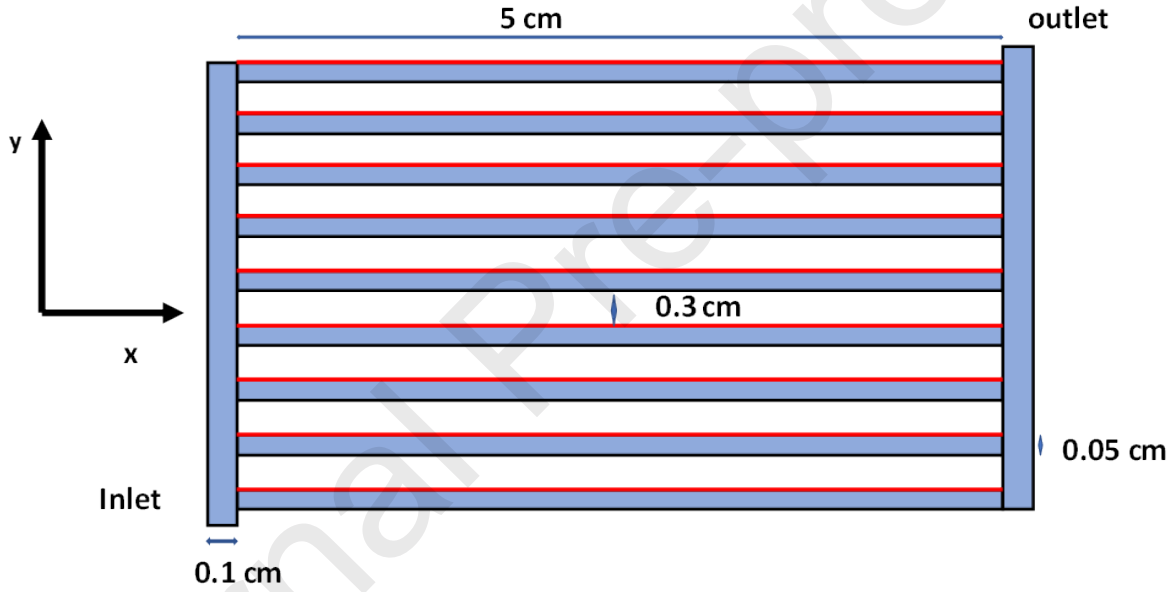

Figure 4. Schematic showing the **(A)** diagram equivalent to the experimental set-up, **(B)** model domains set up in COMSOL Multiphysics for simulation, having the catalytic side (red colour) parallel to the x-direction in 2D.

The velocity and pressure profile in the microreactor were modelled using the Navier-Stokes' equation for Newtonian-incompressible flow (eq. (13)) with no slip boundary conditions on the

stationary wall (i.e. zero velocity at the walls). A laminar inflow rate of 396 $cm^3\ h^{-1}$ was set at the inlet, while the outlet of the microreactor was set at atmospheric pressure.

$$\rho(\boldsymbol{u}\cdot\nabla)\boldsymbol{u} = \nabla\cdot\left[-p\boldsymbol{I}+\mu\left(\nabla\boldsymbol{u}+(\nabla\boldsymbol{u})^{T'}\right)\right]+\boldsymbol{F} \quad (13)$$

where ρ (kg m^{-3}) is the density, $\boldsymbol{u}$ (m s^{-1}) the velocity vector, p (Pa) the pressure, I (dimensionless) is the identity matrix, μ (kg m^{-1} s^{-1}) the dynamic viscosity, T' the transpose operator and F (N m^{-3}) the generic body forces.

Transport in the bulk was described by unsteady state equation (see eq. 14) for diffusion-convection, and isothermal condition was assumed. This equation is embedded in the transport of dilute species node in COMSOL Multiphysics.

$$\frac{\partial C}{\partial t}+\nabla\cdot(-D\nabla C+C\mathbf{u})=0 \quad (14)$$

where D (10^{-9} m^2 s^{-1} was used) is the diffusivity of the 4-nitrophenol in solution. Four boundary conditions and one initial condition are needed to solve for bulk concentration profile. Two of the boundary conditions were drawn from the global boundary, which include the inlet and outlet conditions, while the remaining were local boundary conditions (side walls of each microchannel). At the microreactor inlet, the concentration was also specified as C_t (see eq. (15)) and at the outlet diffusive flux was set to zero (eq. (16)). At the walls with no photocatalyst, the total flux was set to zero (eq. 17), while for the wall with N-TiO_2/rGO film in each microchannel, the total flux towards the surface was set equal to the total rate of adsorption or degradation depending on the condition (eq. (18)).

$$C(t,0,0) = C_t \quad (15)$$

$$-\mathbf{n}\cdot(-D\nabla C)=0 \quad (16)$$

$$-\mathbf{n}\cdot(-\mathrm{D}\nabla C + C\mathbf{u}) = 0 \quad (17)$$

$$-\mathbf{n}\cdot(-\mathrm{D}\nabla C + C\mathbf{u}) = \mathrm{R(dark,light)} \quad (18)$$

Where ***n*** is the normal vector to the surface and C_t is the 4-nitrophenol concentration in the recirculating tank. The initial condition is given by the initial concentration of 4-nitrophenol at time t = 0 (see eq. (19)). With these conditions the bulk concentration profile of 4-nitrophenol can be obtained as a function of x, y, and t in the microreactor.

$$\mathrm{C(0,x,y)} = C_o \quad (19)$$

4-Nitrophenol surface concentration C_s (mol m^{-2}) was calculated as shown in eq. (20), which includes diffusion and reaction rates as previously employed by ref. [12].

$$\frac{\partial C_S}{\partial \mathrm{t}} + \nabla\cdot(-\mathrm{D}_s\nabla \mathrm{C}_S) = \mathrm{R(dark,light)} \quad (20)$$

where D_s is the surface diffusivity of 4-nitrophenol in $m^2\ s^{-1}$, and *R(dark, light)* in mol $m^{-2}\ h^{-1}$ (eq. 21) is the reaction rate for dark adsorption or degradation. The initial condition in eq. (22) is sufficient to solve for the surface concentration profile.

$$\mathrm{R(dark,light)} = \begin{cases} \mathrm{R_{ads}},\ \mathrm{t} \le \mathrm{t_{eq}(dark)} \\ \mathrm{R_s},\ \mathrm{t} > \mathrm{t_{eq}(light)} \end{cases} \quad (21)$$

where t_{eq} is the time needed to reach the adsorption equilibrium and when the solar irradiation simulator was switched on.

$$\mathrm{C}_S\mathrm{(0,x,catalyst\ wall)} = 0 \quad (22)$$

The transport equations in eq. (14) and (20) had previously been used by ref. [10–12,24] to model the degradation of salicylic acid in a photocatalytic microreactor with a single rectangular

microchannel. It is worthy of note that the developed model herein is strictly transport-based and we did not include any radiation model since the experiment was run at a constant light intensity.

3.3.3 Recirculation tank equation

It had been previously reported by Shiraishi et al. [25] that recirculation mode is compatible with photocatalytic reaction because it reduces film-diffusional resistance. Therefore, recirculation was incorporated by setting up eq. (23), which is a mole balance on the recirculation tank. The recirculation model was coupled with eq. (14) through the global boundary condition in eq. (15). The disappearance (C/C_o) of 4-nitrophenol was monitored at regular intervals by sampling from the recirculation tank. It was assumed that: (i) the solution in the tank was effectively mixed at every point in time as in a continuous stirred tank reactor (CSTR); (ii) the volume of the tank is approximately constant as the sampling volume is extremely small and there is no drastic variation in the volume of the 4-nitrophenol solution in the tank. An initial condition is needed to solve eq. (24):

$$\mathrm{V_t}\frac{\mathrm{dC_t}}{\mathrm{dt}} = \mathrm{Q} \times (\mathrm{average}(\mathrm{C_{exit}}) - \mathrm{C_t}) \quad (23)$$

$$\mathrm{C_t}(0) = \mathrm{C_o} \quad (24)$$

where V_t (m^3) and C_t (mol m^{-3}) are the total volume and the concentration of 4-nitrophenol solution in the tank, C_{exit} (mol m^{-3}) is the average concentration of 4-nitrophenol at the microreactor exit and Q ($cm^3\ h^{-1}$) is the specified recirculation flow rate of the pump.

By and large, the unknown variables and the model parameters include C, C_s, $k_{ads,\ m}$, $k_{des,\ m}$, $k_{ads,\ n}$, $k_{des,\ n}$ and k_s: to solve for these variables, the parameters used in the model are summarized in Table 4. The initial concentration, volumetric flow rate, volume of solution were the same as

the ones used in the experiment, and the microreactor dimensions used were the ones provided by the manufacturer.

Table 4. Parameters specified for simulation in COMSOL Multiphysics.

Parameter	Value	Description
C_o	0.0323, 0.0518, 0.134, 0.324 mol m^{-3}	Initial 4-nitrophenol concentration
Q	396 cm^3 h^{-1}	Recirculation flow rate
Γ	8.3106 x 10^{-6} mol m^{-2}	maximum monolayer site concentration
V_t	125 cm^3	Volume of 4-nitrophenol solution
h	0.05 cm	Microchannel width or height
L	5 cm	Microchannel Length
Collector width	0.1 cm	-
Microchannel spacing	0.3 cm	-

3.4 CFD model Results

3.4.1 Velocity distribution in microchannels

Figure 5 shows the velocity profile in all of the nine microchannels, it is evident that the profile follows a gaussian distribution as expected. The profile showed moderate level of flow maldistribution which is typical of parallel microchannels of Z-type configuration [26]. The microchannels closer to the outlet have higher velocity values than the microchannels closer to

the inlet. Overall, the velocity profile in the microchannels is laminar (*Re* = 21) and flow maldistribution levels are minimal.

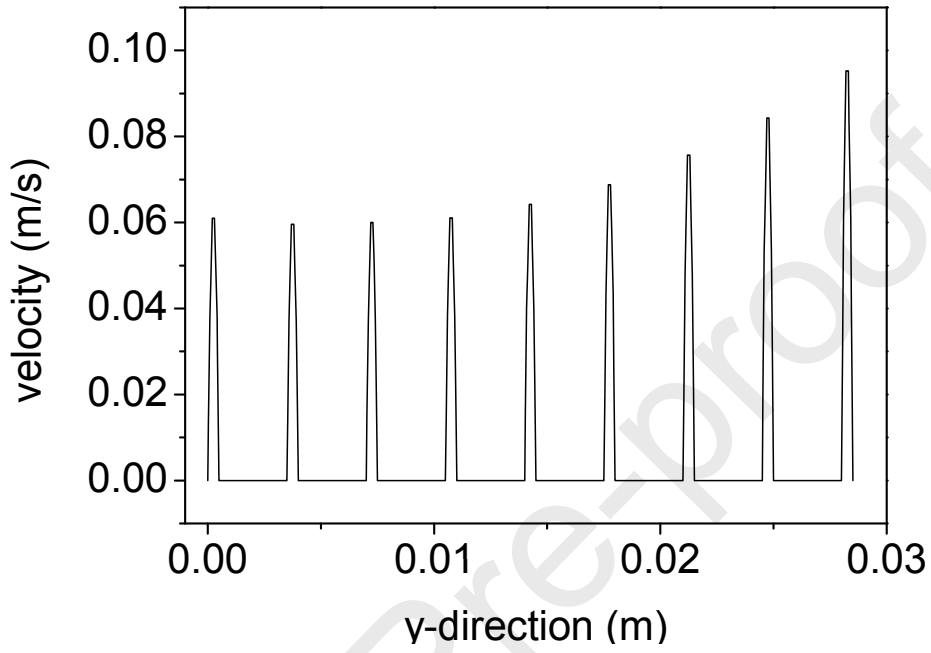

Figure 5. Velocity profile in each of the microchannels at x = 0.03 m (condition: x-direction here is as depicted in Figure 4B).

3.4.2 Concentration distribution

Figure 6 shows the concentration gradient of 4-nitrophenol (C_o = 0.0323 mol m^{-3}) in a microchannel along y-direction (perpendicular to the N-TiO_2/rGO film – see Figure 4B) at x = 3cm, within 1 h of dark adsorption. Evidently there is a concentration gradient between the bulk and the N-TiO_2/rGO film, and diffusion is towards the film surface. The profile becomes flatter as the recirculation time increases and concentration in the microchannels is almost uniform. This does

not correspond to the adsorption time in the recirculation tank, it took longer to reach equilibrium based on the concentration of 4-nitrophenol in the tank.

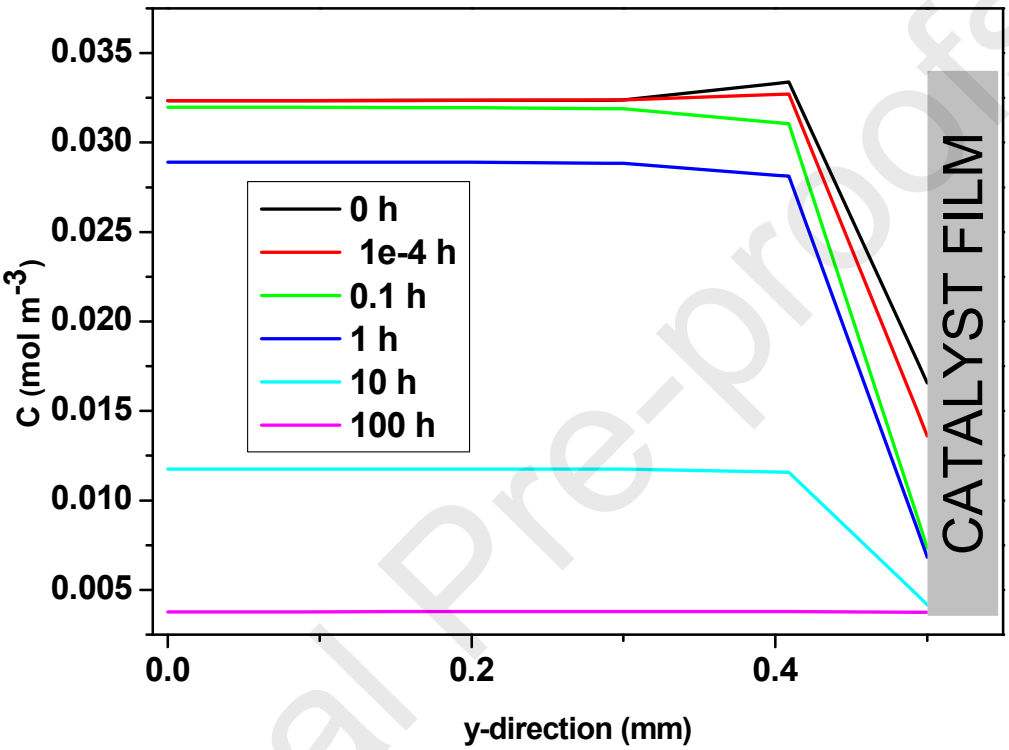

Figure 6. Concentration profile of 4-nitrophenol in the y-direction in a microchannel within 100 h of dark adsorption (conditions: C_o = 0.0323 mol m^{-3} at x = 0.03 m; y = 0 m represents the side of the microchannel without catalyst and y = 0.5 mm represents the side with N-TiO_2/rGO film; y-direction is depicted in Figure 4B).

3.4.3 Validation of CFD model with experimental data

Figure 7 presents the comparison of experimental results to that of the CFD model for initial concentrations of 4-nitrophenol of 0.0323, 0.0518, 0.134, and 0.324 mol m^{-3}. Table 5 shows the optimal estimated parameter for this study while fitting the experiment to model results. From

Figure 7, it can be observed that there is a sharp initial decrease in the concentration of 4-nitrophenol in the recirculation tank in the first 6 h of operation, and about 70 % (on the average) of the 4-nitrophenol had been adsorbed. After 6 h of dark, adsorption rate slowed down and adsorption equilibrium time increased; this trend was observed for all C_o. On the average, about 85 – 90 % of 4-nitrophenol was adsorbed in the dark before degradation, making the degradation rate slower. It is worthy of note that the N-TiO_2/rGO film used in this study is highly porous thereby leading to significant adsorption. The use of compact non-porous film typically results in minor or negligible dark adsorption and greater degradation rate as reported in literature [12,27]. In Figure 7, the model and experimental results are in good agreement comparing the equilibrium concentration in the dark and the final concentration after irradiation with the initial concentration of 4-nitrophenol. The runs at 0.0518 and 0.134 mol m^{-3} showed less amount of deviation compared to the 0.0323 and 0.324 mol m^{-3} ones. This might be because of similar adsorption equilibrium time of 288 h for the former concentrations and significant difference in the values (180 h and 312 h respectively) for the later concentrations. Overall, similar trend can be observed for all C_o initially, slight deviation began to set in the final conversion part.

It can be argued that the 2D model is not absolutely accurate and a three-dimensional model might increase the accuracy but it will be at the expense of computational cost. Nonetheless, we believe that this model is simple, fast and effective for the estimation of intrinsic photocatalytic reaction constant for pollutant degradation in a photocatalytic microreactor operating in continuous recirculation mode under a standardized simulated solar radiation. It is difficult to benchmark our results to previous studies due to the very different nature of catalytic film, microreactor configuration and operation mode utilized. Future outlook will target the applicability of this model in wide range of operating conditions. Although the quantity of

wastewater treated can be small and challenges practical implementation, scaling up by numbering up of this microreactor can help to increase the amount of wastewater to be treated and reduce the operation time. Moreover, this treatment can be seen as a tertiary step in which trace amount of pollutant recalcitrant to biological treatments can be abated.

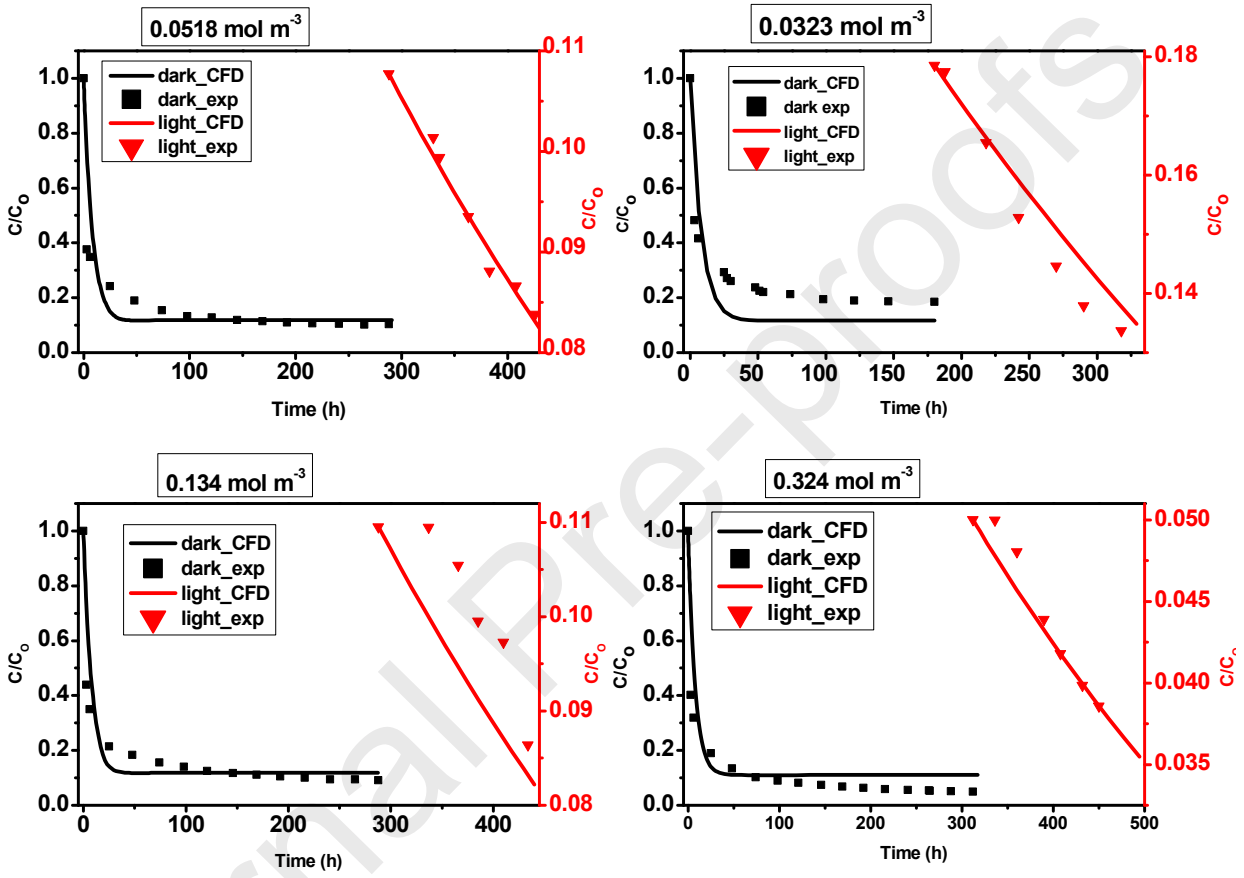

Figure 7. Comparison of the experimental data and model prediction of concentration of 4-nitrophenol in the recirculating tank with different initial concentrations of 0.0323, 0.0518, 0.134, and 0.324 mol m^{-3} (condition: volumetric flow rate = 396 cm^3 h^{-1}, volume of solution in tank = 125 cm^3).

Table 5. Estimated adsorption and degradation parameter (at 396 cm^3 h^{-1} and C_o = 0.0323, 0.0518, 0.134, and 0.324 mol m^{-3}).

$k_{ads,\,m}$ (m^3 mol^{-1} h^{-1})	$k_{des,\,m}$ (h^{-1})	$k_{ads,\,n}$ (m^3 mol^{-1} h^{-1})	$k_{des,\,n}$ (h^{-1})	k_s (h^{-1})
1.76×10^4	0.0252	1.76×10^4	0.0126	2.02

4. Conclusions

A simple and robust CFD model has been proposed and validated for effective prediction of photo-degradation of 4-nitrophenol in a photocatalytic micro-reactor implementing N-TiO_2/rGO film and operating in continuous flow-recirculation mode. The photocatalytic reaction, under the experimental conditions used, shows a really significant dark adsorption due to the high porosity of the film thereby slowing down the degradation rate. The degradation rate of 4-nitrophenol in the microreactor is observed to be proportional to the C_{eq} allowing a simple estimation of the rate constants. The fitting of the experimental results to the model allows the estimation of the kinetic constants for 4-nitrophenol degradation. The model is general enough to predict degradation of most organic pollutant in (waste)water. Although improvements can still be made to the proposed model and the used reactor is a small bench type whose performance cannot be analysed from an economic point of view, we believe that scaling-up, designing, modelling and optimization of appropriate microreactors for photocatalytic processes in (waste)water treatment applications can find a practical use in the near future. The application of the proposed model to a wide range of operating conditions and other photocatalytic processes is a future outlook.

5. Acknowledgments

This work is funded by Abu Dhabi Department of Education and Knowledge (ADEK), Abu Dhabi, United Arab Emirates. Authors would also like to thank Maya Malakian and Lakshmi Satish for her assistance in the Laboratory.

6. References

[1] X. Liu, J. Iocozzia, Y. Wang, X. Cui, Y. Chen, S. Zhao, Z. Li, Z. Lin, Noble metal-metal oxide nanohybrids with tailored nanostructures for efficient solar energy conversion, photocatalysis and environmental remediation, Energy Environ. Sci. 10 (2017) 402–434. doi:10.1039/c6ee02265k.

[2] T.S. Natarajan, K.R. Thampi, R.J. Tayade, Visible light driven redox-mediator-free dual semiconductor photocatalytic systems for pollutant degradation and the ambiguity in applying Z-scheme concept, Appl. Catal. B Environ. 227 (2018) 296–311. doi:10.1016/j.apcatb.2018.01.015.

[3] N. Selvakumar, A. Biswas, S.B. Krupanidhi, H.C. Barshilia, Enhanced optical absorption of graphene-based heat mirror with tunable spectral selectivity, Sol. Energy Mater. Sol. Cells. 186 (2018) 149–153. doi:10.1016/j.solmat.2018.06.041.

[4] R. Gorges, S. Meyer, G. Kreisel, Photocatalysis in microreactors, J. Photochem. Photobiol. A Chem. 167 (2004) 95–99. doi:10.1016/j.jphotochem.2004.04.004.

[5] I. Rossetti, Continuous flow (micro-)reactors for heterogeneously catalyzed reactions: Main design and modelling issues, Catal. Today. 308 (2018) 20–31. doi:10.1016/j.cattod.2017.09.040.

[6] J. Parmar, S. Jang, L. Soler, D.P. Kim, S. Sánchez, Nano-photocatalysts in microfluidics, energy conversion and environmental applications, Lab Chip. 15 (2015) 2352–2356. doi:10.1039/c5lc90047f.

[7] A. Yusuf, C. Garlisi, G. Palmisano, Overview on microfluidic reactors in photocatalysis: Applications of graphene derivatives, Catal. Today. 315 (2018) 79–92. doi:10.1016/j.cattod.2018.05.041.

[8] A. Tanimu, S. Jaenicke, K. Alhooshani, Heterogeneous catalysis in continuous flow microreactors: A review of methods and applications, Chem. Eng. J. 327 (2017) 792–821. doi:10.1016/j.cej.2017.06.161.

[9] G. Charles, T. Roques-Carmes, N. Becheikh, L. Falk, J.-M. Commenge, S. Corbel, Determination of kinetic constants of a photocatalytic reaction in micro-channel reactors in the presence of mass-transfer limitation and axial dispersion, J. Photochem. Photobiol. A Chem. 223 (2011) 202–211. doi:10.1016/j.jphotochem.2011.08.019.

[10] S. Corbel, G. Charles, N. Becheikh, T. Roques-Carmes, O. Zahraa, Modelling and design of microchannel reactor for photocatalysis, Virtual Phys. Prototyp. 7 (2012) 203–209. doi:10.1080/17452759.2012.708837.

[11] S. Corbel, N. Becheikh, T. Roques-Carmes, O. Zahraa, Mass transfer measurements and modeling in a microchannel photocatalytic reactor, Chem. Eng. Res. Des. 92 (2014) 657–662. doi:10.1016/j.cherd.2013.10.011.

[12] S. Corbel, F. Donat, R. Schneider, Kinetic study of photocatalytic degradation of Ifos famide in a microchannel and simulation, SDRP J. Nanotechnol. Mater. Sci. 2 (2019) 1–10. doi:10.25177/JNMS.2.1.RA.452.

[13] L.Y. Ozer, Y. Shin, A. Felten, H. Oladipo, O. Pikuda, C. Muryn, C. Casiraghi, G. Palmisano, Growing N-doped multiphase TiO_2 nanocomposites on reduced graphene oxide: Characterization and activity under low energy visible radiation, J. Environ. Chem. Eng. 5 (2017) 5091–5098. doi:10.1016/j.jece.2017.09.042.

[14] L.Y. Ozer, H. Apostoleris, F. Ravaux, S.I. Shylin, F. Mamedov, A. Lindblad, F.O.L. Johansson, M. Chiesa, S. Jacinto, G. Palmisano, Long-Lasting Non-hydrogenated Dark Titanium Dioxide: Medium Vacuum Anneal for Enhanced Visible Activity of Modified Multiphase Photocatalysts, ChemCatChem. 10 (2018) 2949–2954. doi:10.1002/cctc.201800097.

[15] S. Odiba, M. Olea, Computational Fluid Dynamics in Microreactors Analysis and Design: Application to Catalytic Oxidation of Volatile Organic Compounds, J. Chem. Eng. Process Technol. 07: 297 (2016). doi:10.4172/2157-7048.1000297.

[16] H. Jensen, K.D. Joensen, J.E. Jørgensen, J.S. Pedersen, E.G. Søgaard, Characterization of nanosized partly crystalline photocatalysts, J. Nanoparticle Res. 6 (2004) 519–526. doi:10.1007/s11051-004-1714-3.

[17] M.N. Iliev, V.G. Hadjiev, A.P. Litvinchuk, Raman and infrared spectra of brookite (TiO_2): Experiment and theory, Vib. Spectrosc. 64 (2013) 148–152. doi:10.1016/j.vibspec.2012.08.003.

[18] O. Pikuda, C. Garlisi, G. Scandura, G. Palmisano, Micro-mesoporous N-doped brookite-rutile TiO_2 as efficient catalysts for water remediation under UV-free visible LED radiation, J. Catal. 346 (2017) 109–116. doi:10.1016/j.jcat.2016.12.010.

[19] H. Scott Fogler, Elements of chemical reaction engineering (1987). doi:10.1016/0009-2509(87)80130-6.

[20] P. Davit, G. Martra, S. Coluccia, Photocatalytic Degradation of Organic Compounds on TiO_2 Powders-FT-IR Investigation of Surface Reactivity and Mechanistic Aspects-, J. Japan Pet. Inst. 47 (2004) 359–376. doi:10.1627/jpi.47.359.

[21] A. Sclafani, J.M. Herrmann, Comparison of the photoelectronic and photocatalytic activities of various anatase and rutile forms of titania in pure liquid organic phases and in aqueous solutions, J. Phys. Chem. 100 (1996) 13655–13661. doi:10.1021/jp9533584.

[22] M.L. Satuf, J. Macagno, A. Manassero, G. Bernal, P.A. Kler, C.L.A. Berli, Simple method for the assessment of intrinsic kinetic constants in photocatalytic microreactors, Appl. Catal. B Environ. 241 (2019) 8–17. doi:10.1016/j.apcatb.2018.09.015.

[23] F.B. Scheufele, A.N. Módenes, C.E. Borba, C. Ribeiro, F.R. Espinoza-Quiñones, R. Bergamasco, N.C. Pereira, Monolayer–multilayer adsorption phenomenological model: Kinetics, equilibrium and thermodynamics, Chem. Eng. J. 284 (2016) 1328–1341. doi:10.1016/j.cej.2015.09.085.

[24] E. Sani, J.P. Vallejo, D. Cabaleiro, L. Lugo, Functionalized graphene nanoplatelet-nanofluids for solar thermal collectors, Sol. Energy Mater. Sol. Cells. 185 (2018) 205–209. doi:10.1016/j.solmat.2018.05.038.

[25] F. Shiraishi, M. Nagano, S. Wang, Characterization of a photocatalytic reaction in a continuous-flow recirculation reactor system, J. Chem. Technol. Biotechnol. 81 (2006) 1039–1048. doi:10.1002/jctb.1526.

[26] V. Manoj Siva, A. Pattamatta, S.K. Das, Investigation on flow maldistribution in parallel microchannel systems for integrated microelectronic device cooling, IEEE Trans. Components, Packag. Manuf. Technol. 4 (2014) 438–450. doi:10.1109/TCPMT.2013.2284291.

[27] M. Vaqueiro-Contreras, C. Bartlam, R.S. Bonilla, V.P. Markevich, M.P. Halsall, A. Vijayaraghavan, A.R. Peaker, Graphene oxide films for field effect surface passivation of silicon for solar cells, Sol. Energy Mater. Sol. Cells. 187 (2018) 189–193. doi:10.1016/j.solmat.2018.08.002.

- Photocatalytic degradation of 4-nitrophenol in microreactor under solar irradiation
- The used CFD model incorporates total recirculation mode of operation
- The CFD model accounts for adsorption in the dark
- The CFD model predicts experimental data in a wide range of reactant concentrations